Indian Journal of Engineering & Materials Science
Vol. 21, August 2014, pp. 358-370

Photovoltaic based three-phase four-wire series hybrid active power filter for power quality improvement

M Vijayakumar[a] * & S Vijayan[b]

[a]Department of Electrical and Electronics Engineering, K S R College of Engineering, Tiruchengode 637 215, India

[b]Surya Engineering College, Erode 638 107, , India

Received 20 February 2013; accepted 23 May 2014

This paper proposes a photovoltaic (PV) and battery interfaced series hybrid active power filter (SHAPF), which consists of series active power filter and an LC shunt passive filter. The main benefits of the proposed system provide the compensation against the voltage harmonics, current harmonics and voltage interruption for the whole day. A series active power filter (SAPF) demands a source of energy for compensating the voltage sag/swell. The proposed topology utilizes the green energy source with an energy storage unit to meet the DC-link voltage requirement of the SAPF. The control strategy is based on the dual formulation of the compensation system principles with adaptive fuzzy logic controller (AFLC). In addition the new coordination logic control is proposed to provide the continuous harmonics compensation and outage compensation at the different conditions. The simulation and experimental studies are carried out to validate the effectiveness of the proposed PV interfaced three-phase four-wire SHAPF.

Keywords: Photovoltaic systems, DC-DC boost converter, Voltage source inverter, Total harmonic distortion, Series hybrid active power filter

Power quality (PQ) is an important problem, a power system has to handle for providing its consumers a reliable and economical power supply. Three-phase four-wire (3P4W) distribution systems have been widely used in commercial and industrial installations. In the 3P4W distribution systems, the neutral current carries the zero sequence current due to unbalanced loading among the phase conductors. Due to the tremendous development in the area of power electronics, most of the industrial and commercial loads possess non-linear characteristics; such loads are computers, lighting ballasts, switched mode power supply, motor drive applications etc. These loads are the major source for introducing harmonics in the supply current as well as excessive neutral current.

To improve the power quality, different solutions have been proposed by different authors. Among them the shunt and series active power filters have proven as an important and flexible alternative solution to compensate voltage and current related power quality problems in the distribution system[1-4]. Different series APF and SHAPF topologies are used by many researchers such as, for example, three-phase three-leg (3P3L) voltage source inverter (VSI) with split capacitor and a three-phase four-leg (3P4L) VSI for the series APF[5-8] for enhancing electric power quality. The series APF systems need certainty to provide active power into the power system to maintain the load voltage level during voltage sag. At the same time, the power flow in the series APF system has drastically increased during the source voltage sag. Thus, additional energy sources need to be added into series APF system DC-link. Dasgupta *et al.*[9,10] proposed the single-phase and three-phase series APF interfaced with the renewable energy systems with energy storage device to facilitate a specific amount of active power flow from renewable energy source to the load irrespective of the microgrid voltage condition. The unified power quality conditioner (UPQC) is another alternative device used to eliminate both the voltage and current related power quality problem, but implementation of UPQC is an expensive solution[10-12].

The SHAPF system is proposed to compensate the harmonics and reactive power in 3P4W distribution system, it is a combination of a shunt passive filter and a series active power filter. The shunt passive

*Corresponding author (Email: mvijayksrce@gmail.com)

filter suppresses the prevalent harmonics currents produced by the load, while the series active filter connected in series with the source acts as a "harmonic isolator" between the source and the load. It also compensates the reactive power, neutral current reduction and also balances asymmetrical loads. The conventional systems, which are supported by DC-link capacitor/battery bank, can provide large amounts of instant active power to mitigate unbalanced voltage sag for a limited time duration[13-15]. The conventional SHAPF system cannot compensate the long-term power quality problems. The proposed PV and battery bank interfaced DC-DC converter operated SHAPF system provides compensation against long-term voltage sag, swell, interruption, harmonics and reactive power. The aim of this paper is to enhance the voltage and current based compensation capability of the proposed 3P4W SHAPF system with an extended reference signal generation method with the use of the AFLC. In addition the new coordinating logic is proposed to perform various operating modes to manage the different state of affairs.

The control schemes based on fuzzy logic, neural networks and adaptive techniques are helpful for modeling and/or controlling systems characterized by uncertainties and nonlinearities. Fuzzy logic control application to power systems has been a dynamic research area for the past 2 decades, such as for example FLC utilized for electrical drives, shunt active filter and UPQC topologies[16-18]. In this paper, an AFLC is applied to the control of the series APF. The AFLC ensures exact tracking of the reference signals and is robust against parameter uncertainty and disturbances acting on the power system.

The performance of the AFLC was examined and compared with a conventional proportional and integral (PI) controller. A simulation and experimental results are presented to demonstrate the effectiveness of the proposed topology.

Design of Series Hybrid Active Power Filter

The proposed scheme of PV based series hybrid active power filter shown in Fig. 1. It consists of PV connected series active power filter, shunt passive filter and typical voltage and current harmonics type of sources. The series active power filter protects the sensitive load from the fluctuation of the supply voltage. It injects the compensation voltage in series with the supply voltage through the coupling transformer and thus considered as a controlled VSI[19,20]. The required DC bus voltage for series active

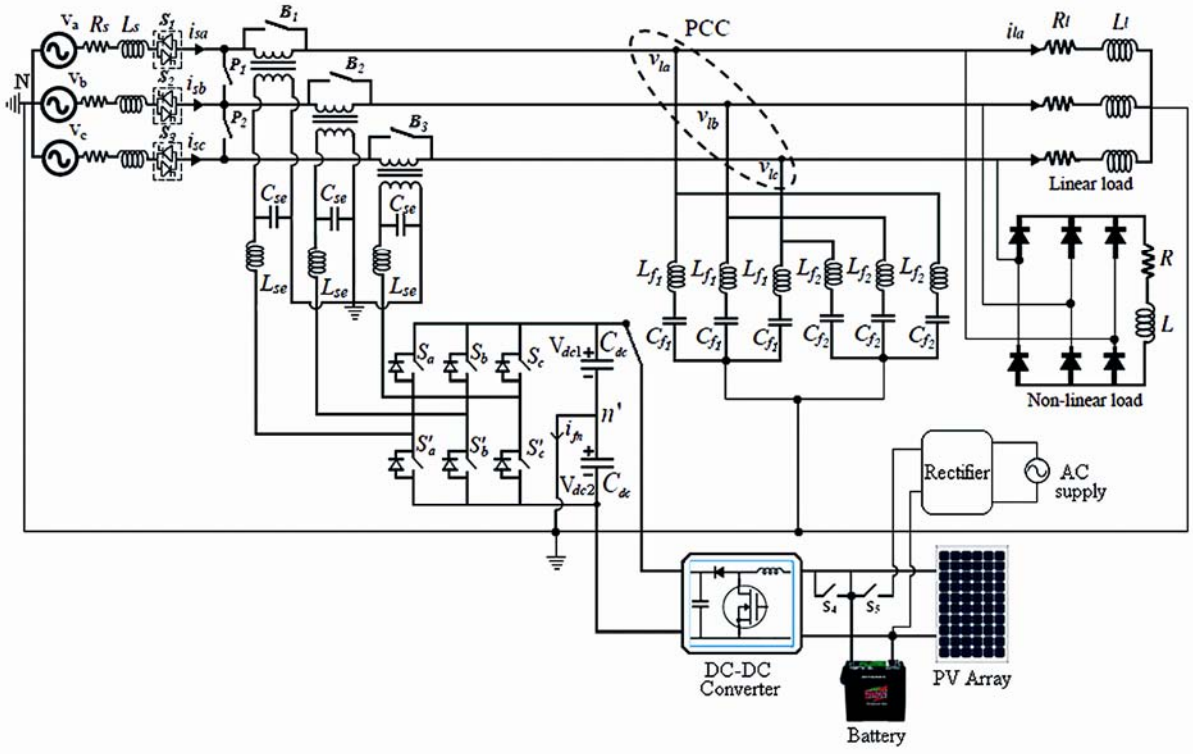

Fig. 1—PV based series active filter with shunt passive filter topology

power filter is provided from the PV array connected with DC-DC boost converter.

The VSI consists of insulated-gate bipolar transistors (IGBTs), inductors and DC capacitors. The value of the DC bus voltage of VSI based hybrid filter compensation mainly depends on the instantaneous energy available to the active filter. Thus, the DC-link capacitor voltage can be maintained at a reference value. However, when the load condition varies, the real power balance between the source and the load will be disturbed. This real power difference will be compensated by DC-link capacitor.

The DC bus voltage is calculated as[21]:

$$V_{dc}=\frac{2\sqrt{2}V_{LL}}{\sqrt{3}m} \quad \ldots (1)$$

where, V_{LL} is the AC line output voltage, m is the modulation index and is considered as 1. The DC capacitor is calculated using the expression,

$$\tfrac{1}{2}C_{dc}\left[\left(V_{dc}^2\right)-\left(V_{dc1}^2\right)\right]=3V\left(\alpha I\right)\mathrm{t} \quad \ldots (2)$$

where, V_{DC} is the reference DC voltage and V_{DCl} is the minimum voltage level of DC bus, α is the overloading factor taken as 1.2 considering 120-180% of steady-state current during transient conditions. V is the phase voltage, I is the phase current, and t is the time at which the DC bus voltage is to be recovered. The calculated value of C_{DC} is 1780 μF, accordingly C_{DC} is chosen to be standard available value nearest to calculated value is 2200 μF.

The *LC* filter unit eliminates the dominant harmonics produced by inverter circuit. The inverter side filter is closer to the harmonic source and low voltage side thus it prevents the harmonic currents to penetrate into the series injection transformers[21].

The selection of the filter inductance (L_{se}) of VSI depends on the current ripple $i_{cr,\ p\text{-}p}$, switching frequency f_s and DC bus voltage (V_{DC}).

The optimum value of thr filter inductance(L_{se}) is expressed as

$$L_{se}=\frac{\sqrt{3}mV_{dc}}{12\alpha f_s i_{cr,p-p}} \quad \ldots (3)$$

Filter capacitance can be expressed as

$$C_{se}=K\frac{V_{dc}}{L_{se}f_s^{\,2}\,i_{cr,p-p}} \quad \ldots (4)$$

where, m is the modulation index, α is the overload factor and K is the filter factor assumed the value is 0.00716.

The series injection transformers not only reduce the voltage requirement of the series inverters, but also provide isolation between the inverters. This can prevent the DC storage capacitor from being shorted through switches in different inverters.The electrical parameters of series injection transformer should be selected correctly to ensure the maximum reliability and effectiveness.

The PV-SHAPF is designed such that, when the PV system generates excess power greater than the load demand, the energy produced by the PV array is used to provide the power to compensation and excess of power is stored in the battery bank. The surplus energy stored in the battery bank is used to regulate the load voltage at night time or when the solar irradiation is unavailable. The coordination logic of the semiconductor switches S_1, S_2, S_3, B_1, B_2, B_3, P_1 and P_2 for different operating modes to handle different situation is given in Table 1.

When the battery is in the charging state during the night or solar irradiation is unavailable, switch S_5 is turned on and a battery charger using a rectifier associated with utility grid is adapted to charge the battery. On the other hand, when the battery in the discharging state during the day/solar irradiation available, only switch S_4 is turned on and battery uses the PV array to charge the battery bank.

The proposed PV-SHAPF operates in three modes of operation. The modes are (i) compensator mode, (ii) voltage interruption/energy conservation mode and (iii) protection mode or idle mode.

Compensator mode

In this mode the proposed PV-SHAPF system is utilized to compensate the voltage and current based distortions and reactive power. During this operating mode a series injection transformer is configured in

Table 1—Control logics of semiconductor switches

Mode	Control signals									
	Series switches					Parallel switches		By pass switches		
	S_1	S_2	S_3	S_4	S_5	P_1	P_2	B_1	B_2	B_3
Compensator mode	1	1	1	1	1	0	0	0	0	0
Voltage interruption /Energy conservation mode	0	0	0	1	0	1	1	0	0	0
Protection mode	1	1	1	0	0	0	0	1	1	1

series with the PCC to compensate the voltage sag/swell. The PV/battery connected DC-DC boost converter manages the DC-link to provide continuity of compensation effectively. The control logic of the compensator mode is given in Table 1.

Voltage interruption/energy conservation mode

During the voltage interruption period or excess power generation on the PV system, the proposed PV-SHAPF disconnects the utility grid from load through the semiconductor switches (S_1, S_2 and S_3). The series injection transformer is reconfigured into parallel by using the semiconductor swiches (P_1 and P_2) to execute the inverter operation to feed the energy generated by the PV array to common load. During low power generation on the PV system, the charge control algorithm reconnects the utility grid and output of the controlled rectifier in parallel with the output of PV array to supply the required power to the batteries and load.

Protection Mode or idle mode

In this mode, the entire PV-SHAPF is disconnected through the semiconductor switches B_1, B_2 and B_3 by bypassing the secondary of an injecting transformer, when the SAPF system needs to protect from the major fault or maintenance.

Photovoltaic Array With DC-DC Boost Converter

The DC-DC boost converter with PV or battery unit is connected in parallel to DC capacitor to maintain the DC link voltage[22,23]. The PV/battery unit with DC-DC boost converter arrangement is shown in Fig. 2. The DC-DC boost converter comprises of a high speed IGBT switch, inductor, diode and capacitor. The output voltage can be controlled by varying the switching duty cycle (D) of the IGBT Q_1. When the IGBT Q_1 is turned on using a pulse width modulation (PWM) generator, current starting flows through L and IGBT Q_1. The energy is stored in the inductor (L), the load current is supplied by the charge in capacitor C.

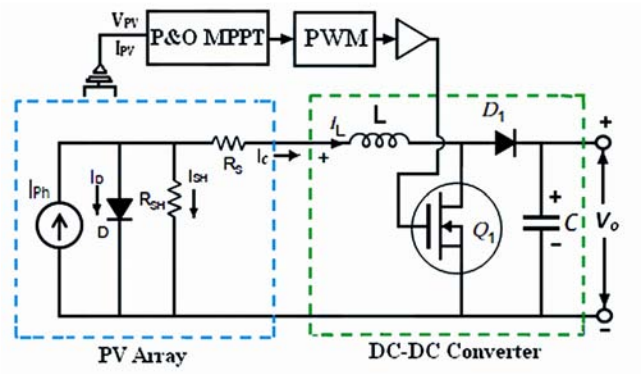

Fig. 2—Topology of PV operated DC-DC boost converter

When the switch IGBT Q_1 is turned off, the inductor voltage adds to the source voltage and current due to this boosted voltage now flows from the source through inductor *L*, diode and the load, which recharges the capacitor *C*. The photovoltaic array/battery voltage is fed to the DC-DC boost converter and the output voltage of this boost converter maintain the DC link voltage of the three-phase VSI.

The selection of the inductance (*L*) of the boost converter depends on the duty cycle (*D*), switching frequency f_s, and R_o is expressed as Ref.[23] The boost converter inductance given by

$$(L) = \frac{R_o * D(1-D)^2}{(2 * f_s)} \quad \ldots (4)$$

where, *D* is the duty cycle = 1- V_{in}/V_{out} =1-36/180=0.8, f_s=25 kHz and R_o is equivalent load resistance =V_o/I_o Ω, thus inductance *L* value obtained as 2.88 µH and it is approximated as standard value as 3 µH.

The capacitor value for the boost converter calculated using the expression

$$C = \frac{V_o * D}{f_s * \Delta V_o * R_o} \quad \ldots (5)$$

where, V_o is the output voltage of the boost converter, ΔV_o is a ripple voltage requirement calculated as 9 V considering voltage ripple factor ($\Delta V_o/V_o$) is 5% thus capacitance value calculated as 142.22 µF and is approximated to standard capacitor value is 150 µF.

Maximum Power Point Tracking Method

In the proposed systems, the solar power produced from the PV array is the main power source, and the battery bank has served as the backup power source. The PV power generating system offers power for the compensation and load when the solar power becomes excessive. During the insufficient power generation, the combination of the battery bank and PV array provides the power for the compensation of power quality disturbances. The perturb & observe (P&O) maximum power point tracking (MPPT) algorithm used in the proposed high step-up DC-DC converter tracks the maximum power point of the PV panel[24,25]. The flow chart of the P&O MPPT algorithm is shown in Fig. 3.

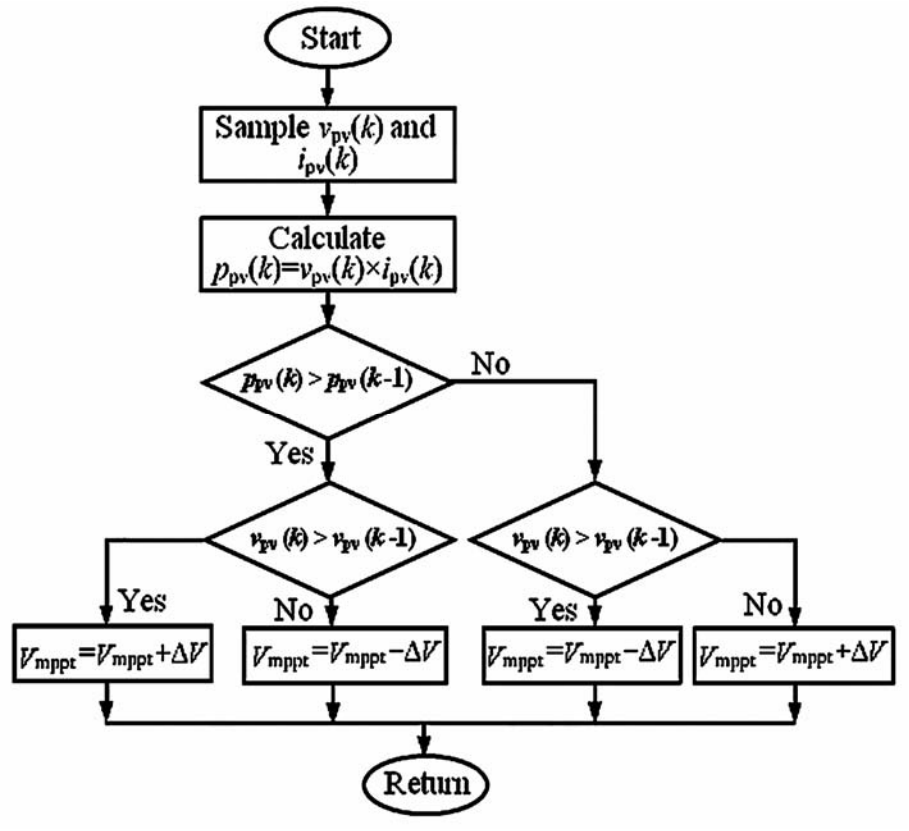

Fig. 3—Flowchart of P&O MPPT algorithm

The output voltage (V_{pv}) of the PV array is compared with a reference voltage which is calculated from the MPPT algorithm to generate the duty cycle required for tracking the maximum power point of the PV array. The control structure of PI controller based P&O MPPT is shown in Fig. 4.

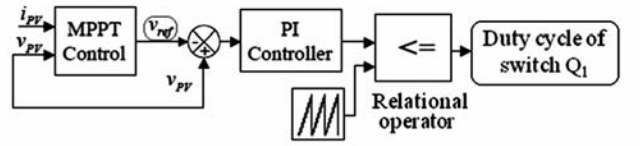

Fig. 4—Control structure of P&O MPPT

Proposed Control Strategy

The power generating system has to handle to provide its consumers a reliable and economical supply with sinusoidal and balanced voltages. Due to this reason objective of the compensation based on an ideal reference load, it must be balanced resistive load with linear characteristics. It means that the source currents are in phase with the supply voltage and the system will have unity power factor. The proposed controller based on the instantaneous power theory with the fuzzy logic controller (FLC) used to control the VSI[26-29]. The point of common coupling (PCC) should follow the linear characteristics, therefore it satisfies the following expression

$$V = \mathrm{R_e}\, i \qquad \ldots (11)$$

where, R_e is the equivalent resistance, V is the voltage vector at the connection point and i is the load current vector.

Voltage and current vectors of three-phase four-wire distribution system can be defined as:

$$v = \begin{bmatrix} v_a & v_b & v_c \end{bmatrix}^T \qquad i = \begin{bmatrix} i_a & i_b & i_c \end{bmatrix}^T \qquad \ldots (12)$$

Balanced resistive load considered as the ideal reference load, when the system currents are unbalanced and non-sinusoidal. The active power supplied by the source is given by

$$P_S = I_1^{+2} R_e \qquad \ldots (13)$$

where, I_1^{+2} is the norm of the positive sequence fundamental component of the current vector, whose average is given by

$$I_1^{+2} = \frac{1}{T}\int_0^T \left(i_1^{+T}.i_1^{+}\right)dt \quad \ldots (14)$$

where, i_1^+ is the positive sequence fundamental component of the instantaneous current vector. Compensator instantaneous power is defined as the difference between the total real instantaneous power required by the load and the instantaneous power supplied by the source.The compensator instantaneous power is stated as

$$P_C = P_L - P_S \quad \ldots (15)$$

where, P_L is the total real instantaneous power required by the load, *Ps* is the instantaneous power supplied by the source. The active power exchanged by the compensator is assumed as null, when the average value is calculated. The following expression satisfies this condition:

$$0 = \frac{1}{T}\int P_L\ dt - I_1^{+2}R_e \quad \ldots (16)$$

The equivalent resistance is given by

$$R_e = \frac{\frac{1}{T}\int P_L\ dt}{I_1^{+2}} = \frac{P_L}{I_1^{+2}} \quad \ldots (17)$$

The load average power (P_L) is given by

$$P_L = \frac{1}{T}\int P_L\ dt = \frac{1}{T}\int v_L^T\ idt \quad \ldots (18)$$

where, v_L^T is the transpose voltage vector at the load side.

The objective is that the compensation equipment and load have an ideal behavior from the PCC. The voltage at the PCC is given by

$$v_{PCC} = \frac{P_L}{I_1^{+2}}i \quad \ldots (19)$$

The reference signal of the active filter to decide the output voltage of the active filter is given by

$$v_C^* = v_{PCC} - v_L = \frac{P_L}{I_1^{+2}}i - v_L \quad \ldots (20)$$

When the active filter supplies the compensation voltage V_c^*, the set load and compensating equipment will behave as a resistor with its equivalent value R_e.The reference signal is determined by the proposed controller. The block diagram of the proposed controller is shown in Fig. 5.

The controller input signals are voltage and current vectors are measured from the load and source side respectively. These current and voltage vectors are multiplied to obtain instantaneous power and load active power is obtained from low pass filter (LPF). In the next stage this instantaneous power is divided by the norm of the positive sequence fundamental component of current vector.

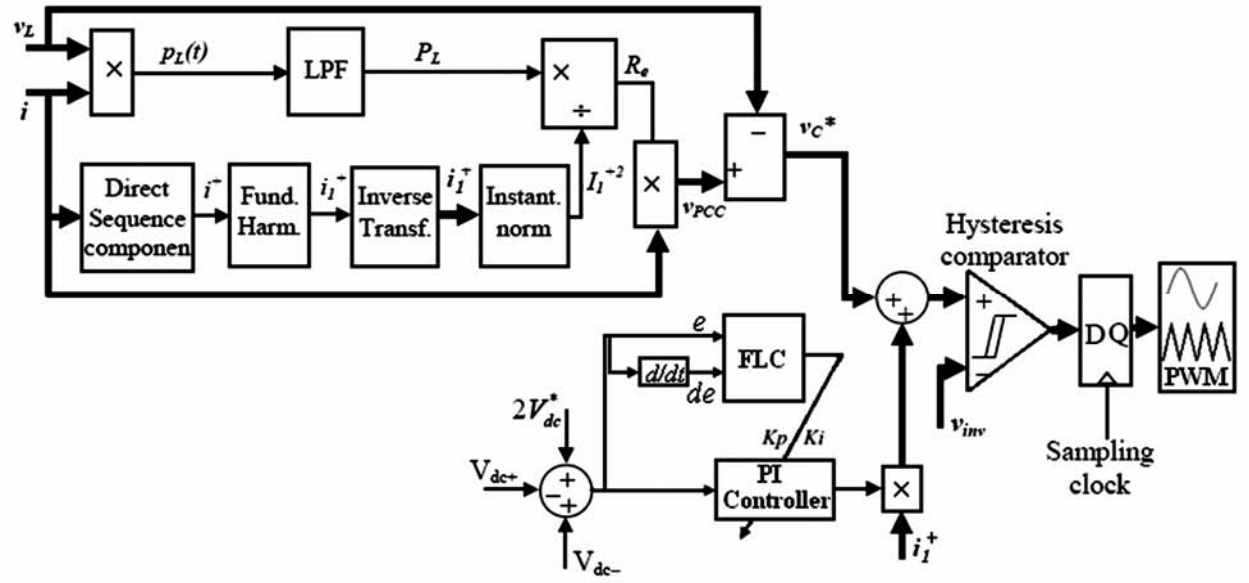

Fig. 5—Block diagram of the proposed controller

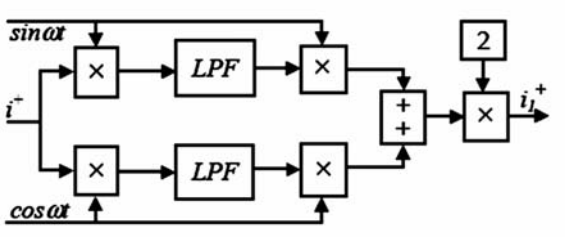

Fig. 6—Fundamental component calculation block

The norm of the positive sequence fundamental component of current vector (I_1^{+2}) is derived from the direct sequence component of the current vector using fundamental component calculation block which is shown in Fig. 6. Each component of the source current vector is multiplied by *sinωt* and *cosωt*, where ω is the fundamental frequency in rad/s. The average values of the results are obtained using two low pass filters. They are multiplied by *sinωt* and *cosωt* again and then by 2. This allows the fundamental harmonic of the current direct sequence component to be obtained.

$$i^{+} = \frac{1}{\sqrt{3}}(i_a + ai_b + a^2 i_c) \quad \ldots (21)$$

where, a operator is defined as $a = e^{j2\pi/3}$, this operator is implemented by an all pass filter.

The Fortescue transformation allows current vector of direct sequence fundamental component to be obtained. It is calculated by way of the expression

$$\vec{i}_1^{+} = \left[i_{1a}^{+} \;\; i_{1b}^{+} \;\; i_{1c}^{+} \right]^T = \left[i_{1a}^{+} \;\; a^2 i_{1a}^{+} \;\; a i_{1a}^{+} \right]^T \quad \ldots (22)$$

where, i_{1a}^{+}, i_{1b}^{+} and i_{1c}^{+} are the fundamental components of the direct sequence current vector. To calculate the norm of i^{+} vector, it is possible to use the Eq. (23) instead of Eq. (14), since $\vec{i}_1^{+}$ vector is a balanced three-phase vector with sinusoidal components.

$$I_1^{+2} = i_{1a}^{+2} + i_{1b}^{+2} + i_{1c}^{+2} \quad \ldots (23)$$

This modified value of the fundamental components of the direct sequence current vector is implemented in the controller block as "instant norm".

In this configuration, two 2200 μF capacitors are connected at the three-phase VSI DC-link as split capacitor topology. While maintaining DC-link voltage constant, APF (active power filter) provides compensated harmonic voltage and reactive power required by the load. In the conventional PWM, the amplitude modulation index is given by

$$m = \frac{V_{ref}}{V_{triangle}} \quad \ldots (24)$$

where, V_{ref} is the amplitude of sinusoidal voltage, and V_{triangle} is the amplitude of triangular carrier voltage. Therefore, the output voltage of the inverter is

$$V_{out} = m * V_{dc} \quad \ldots (25)$$

where, V_{DC} is the DC-link voltage of APF. DC link capacitor helps in reducing noise. However, in the variable non-linear system, DC-link voltage is not constant. Difference between DC-link voltage and reference DC voltage will contain an opposite harmonic component[24,25].

$$V_{error} = V_{dc}^{*} - V_{dc} \quad \ldots (26)$$

where, V_{error} is the difference between reference DC-link voltage (V_{DC}) and APF reference DC-link voltage(V^{*}_{DC}), V_{error} supplies reactive power required by the load and compensating the harmonic voltage. If V_{error} is required a correction for inverter amplitude modulation index, actual index becomes

$$m_{actual} = \frac{V_{error} * V_{ref}}{V_{triangle}} \quad \ldots (27)$$

Therefore,V_{out} becomes given by

$$V_{out} = m_{actual} * V_{dc} \quad \ldots (27)$$

In this proposed control scheme, the AFLC is designed to adjust the PI controller parameters K_p and K_i, to the purpose of reducing some in-built characteristic of the error between the reference and system response. An adaptive controller generally is based on the mechanism ultimately causing the instantaneous selection of the control parameters. In this case, the fuzzy controller is designed to adapt PI parameters K_p and K_i , in order to reduce at least some inherent characteristics (overshoot, response time, etc.) of the error between the reference and system response.The main objective of this AFLC structure is to reduce the control scheme complexity without deriving the mathematical modeling and to keep a

high level of the dynamic performances. The controller inputs are the error (e) and the error derivative (de). The fuzzy controller outputs are K_p and K_i, representing the weights of the proportional and integral actions of the PI controller.

The fuzzy sets were defined for the input and output variables. They are negative (N), zero (Z) and positive (P) for input variables and negative big (NB), negative medium (NM), zero (ZE), positive medium (PM) and positive big (PB) for output variables. The membership functions of the input and output variables are shown in Fig. 7. In this control scheme, the min-max method was used for fuzzification and the defuzzification process was based on the maximum membership principle.

The rule base stores the linguistic (fuzzy number) control rules required by the rule evaluator (decision making logic). The rules used in this control scheme are given in Table 2. The obtained normalized input quantities are crisp in nature, hence it needs to convert to their corresponding fuzzy variables. After the fuzzification process, the fuzzified inputs are given to the fuzzy inference mechanism. The fuzzy inference mechanism gives the control output based on the given fuzzy rule base. This output is converted into actual control outputs K_p and K_i by using the scaling factors.

Table 2—Fuzzy rule base table

e	de	K_i	K_p
N	-	ZE	PB
Z	N	NM	PB
Z	Z	ZE	PM
Z	P	PM	NB
P	-	ZE	PB

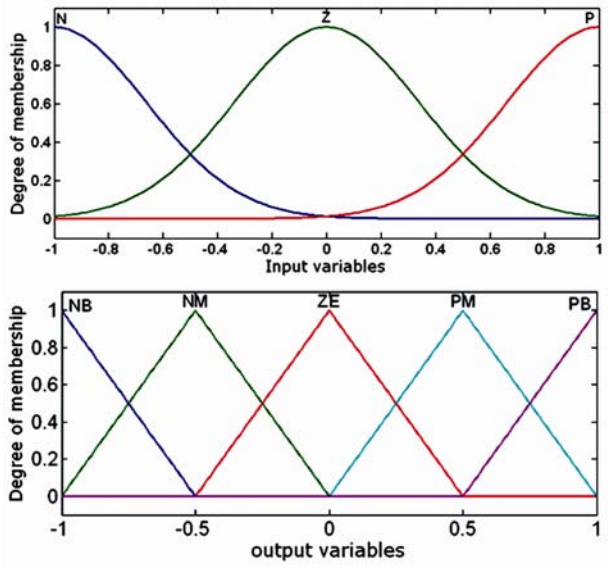

Fig. 7—Membership functions for the input and output variables

This PI controller parameter obtained from the FLC is used in the proposed PI controller to control the DC-link voltage. The output of the PI controller multiplied by i_1^+ and is calculated with the reference voltage V_c^*, through the above function reference voltage and further corrected to accurate value. The PWM technique is used to control the three-phase VSI to generate the compensation voltage. The gating signals are generated by comparing the reference signal (V_c^*) with inverter output voltage (V_{in}) using the hysteresis band.

Simulation Results

In this paper, the proposed fuzzy logic-based instantaneous power theory control algorithm for the PV based SHAPF is evaluated using Matlab/Simulink software under unbalanced and distorted load-current and source-voltage conditions. In the simulation studies, the results are specified before and after the operation of the PV based SHAPF system.

The SHAPF system parameters given in Table 3. For evaluating the performance of the PV-SHAPF under the unbalanced voltages with unbalanced loads, the unbalanced non-linear load is fed by unbalanced AC voltages. The unbalanced source voltages (e_{sabc}), injected voltage, load voltage (V_{labc}) after compensation, unbalanced load currents (i_{labc}), active filter currents (i_{fabc}), source currents (i_{sabc}), source voltage (e_{sa}) superimposed by the source current (i_{sa}), are shown in Fig. 8. The results shown in Fig. 8 confirm that the PV based SHAPF system is able to

Table 3—The SHAPF system parameters

	Parameters		Value
Source	Voltage	V_{Sabc}	110 V
	Frequency	f	50 Hz
DC-link	Voltage	V_{DC}	180 V
	Two series capacitor	C_1,C_2	2200 µF
Series APF	Filter	L_{rf},C_{rf}	12.54 mH, 75 µF
	Switching frequency	f_s	10 kHz
	Injection transformer	T_1,T_2,T_3	N_1/N_2=2,5.4 kVA
Passive filter	LC value	L_5,C_5	12.5 mH, 33 µF
	LC value	L_7,C_7	6.8 mH, 33 µF
Non-linear load	3Φ thyristor rectifier	L_L,L_{DC},R_{DC}	3 mH, 5.7 mH, 12 Ω
Load	RL load	R_L,L_L	7 Ω,75 mH
	kVA rating		5 kVA
PI controller	PI controller gains	K_p, K_i	6,5.5

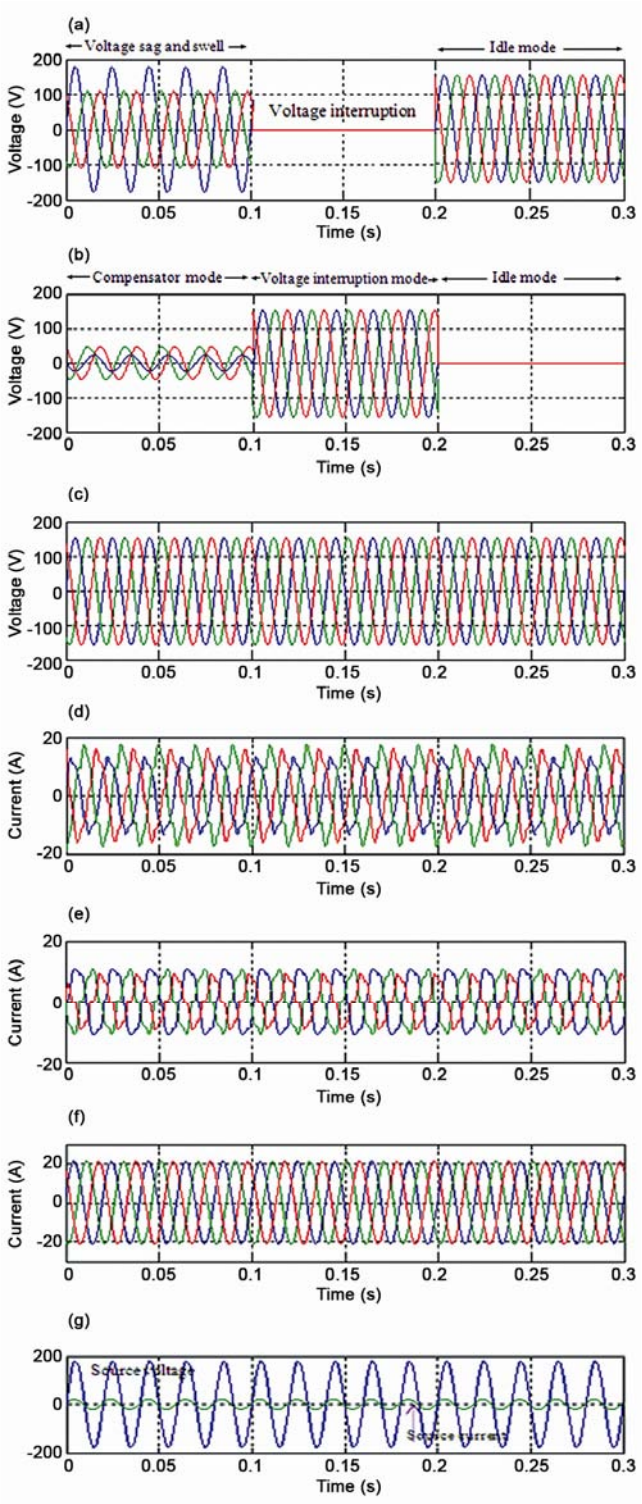

Fig. 8—Simulation results under balanced voltages with unbalanced loads: (a) source voltages (V_{sabc}) before compensation, (b) injected voltage, (c) load voltage (V_{labc}) after compensation, (d) load currents (i_{labc}), (e) active filter currents (i_{fabc}), (f) source currents (i_{sabc}) and (g) source voltage (V_{sa}) superimposed by the source current (i_{sa})

improve the power quality and compensate the load voltage interruption.

Before installing the active power filter, the measured total harmonic distortion (THD) level of the load voltage in phase -A was 23.7% and the source current was 32.1%; after compensation, the THD level of the load voltage is approximately 1.52% and the source current is approximately 3.43% shown in Fig. 9, which is well within the limit specified by IEEE Std. 519-1992[29] . In addition, the source current is in phase with the source voltage, so that the power factor is equal to one as shown in Fig. 8 (g). Figure 10 shows the neutral current before compensation and after compensation, it is evident that effective neutral current compensation of the proposed topology.

Figure 11 shows the variation of solar irradiance, PV array output voltage and DC-link capacitor voltage. Figure 12 shows the discharge characteristic of the battery for various current outputs. From the characteristics, it is observed that the battery can feed 60 A for 8 h duration.

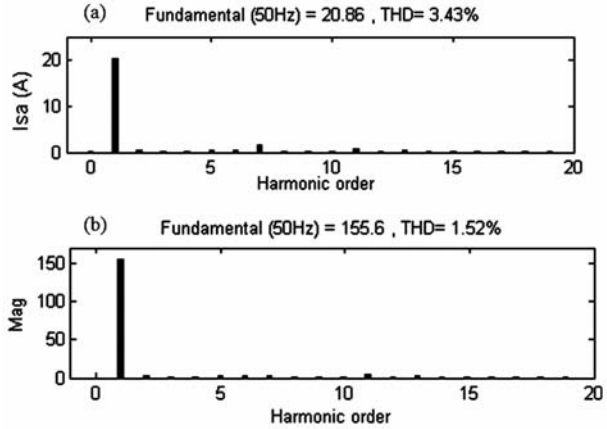

Fig. 9—THD level of source current and load voltage after compensation in phase-'*a*'

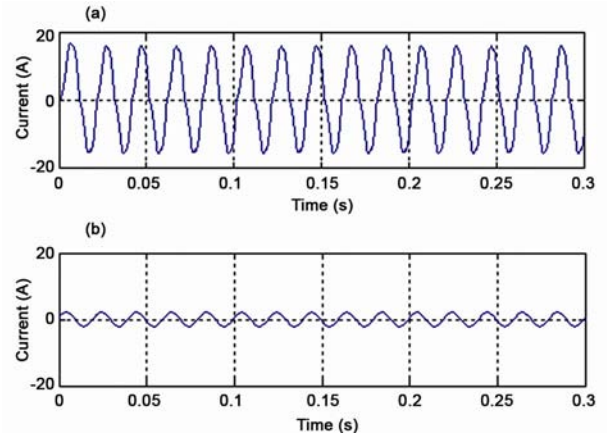

Fig. 10—Neutral current before and after installing SHAPF

Simulation results show that the proposed control strategy compensates harmonic components as well as most of the other unbalanced load current distortion in electric power systems with three-phase four-wire. Finally, the voltage and current harmonic compensation capability of the proposed PV based SHAPF for PI and FLC control methods are shown in Table 4 as simulation results and THD levels.

Table 4—Simulation results and THD levels of voltage and current waveforms at PCC

		Before PV based SHAPF		After PV based SHAPF	
	Phases	Currents (A)	Voltages (V)	Currents (A)	Voltages (V)
THD (%)	A	32.10	23.70	3.43	1.52
	B	29.35	20.50	3.20	1.85
	C	31.70	23.36	3.52	2.15
RMS	A	9.3	126.5	15.3	110.00
	B	13.2	76.99	15.4	110.00
	C	12.3	76.99	15.3	110.10
	N	13.1	--	1.8	--

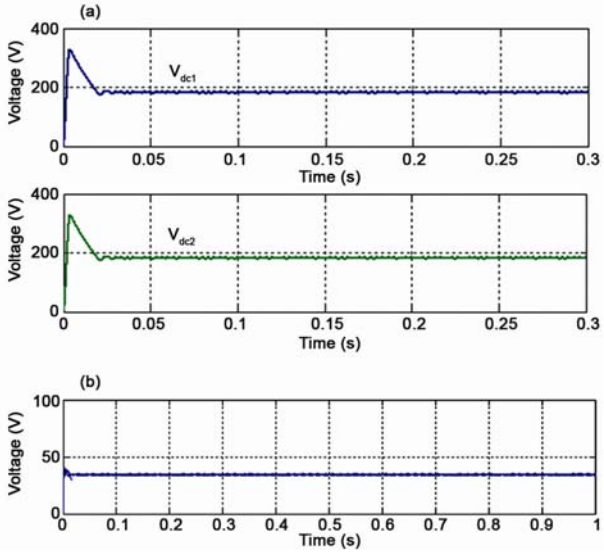

Fig. 11—DC-link capacitor voltage and PV array output voltage

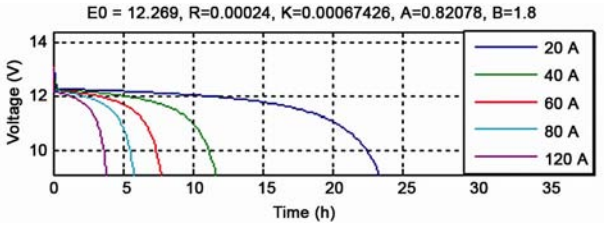

Fig. 12—Discharge characteristics of the battery for various output currents

Experimental Results

The experimental prototype in the three-phase four-wire PV based SHAPF system consists of a voltage source inverter (series APF) and shunt passive filter. The voltage source inverter is connected with DC bus split-capacitor and the dsPIC30F4011 device for controlling the SHAPF system.

The experimental prototype the series APF is connected in series with the line using series coupling transformer. The DC-links of series APFs are connected to two common series 2200 μF DC capacitors under 180 V DC in split capacitor topology. PV connected DC-DC boost converter is connected to the DC-link, in which DC voltage is stored using the DC-link capacitor. A three-phase diode bridge rectifier with RL loads are used as nonlinear loads. All of the prototype circuit parameters and experimental environment are set up nearly the same as the simulation conditions. The experimental results show the close agreement with the simulation results, by which it satisfies the control objectives of the proposed system effectively.

The experimental results carried out under unbalanced voltages with unbalanced load condition. Figure 13 shows the experimental results of the unbalanced source voltages (e_{sabc}), injected voltage, load voltage (V_{labc}) after compensation, unbalanced load currents (i_{labc}), source currents (i_{sabc}), source voltage (e_{sa}) superimposed by the source current (i_{sa}). Figure 14 shows the PV array output voltage, high step-up DC-DC converter output voltage, DC-link capacitor voltage and neutral current after compensation.

The proposed PV-SHAPF is tested during a voltage interruption. The supply voltage of the system is reduced to zero by disconnecting or by switch offing the mains. Figure 15 shows the supply voltage before compensation and load voltage after compensation.

The harmonic order of the source current and load voltage after compensation in phase "*a*" shown in Fig. 16. The THD level of the source currents before compensation are

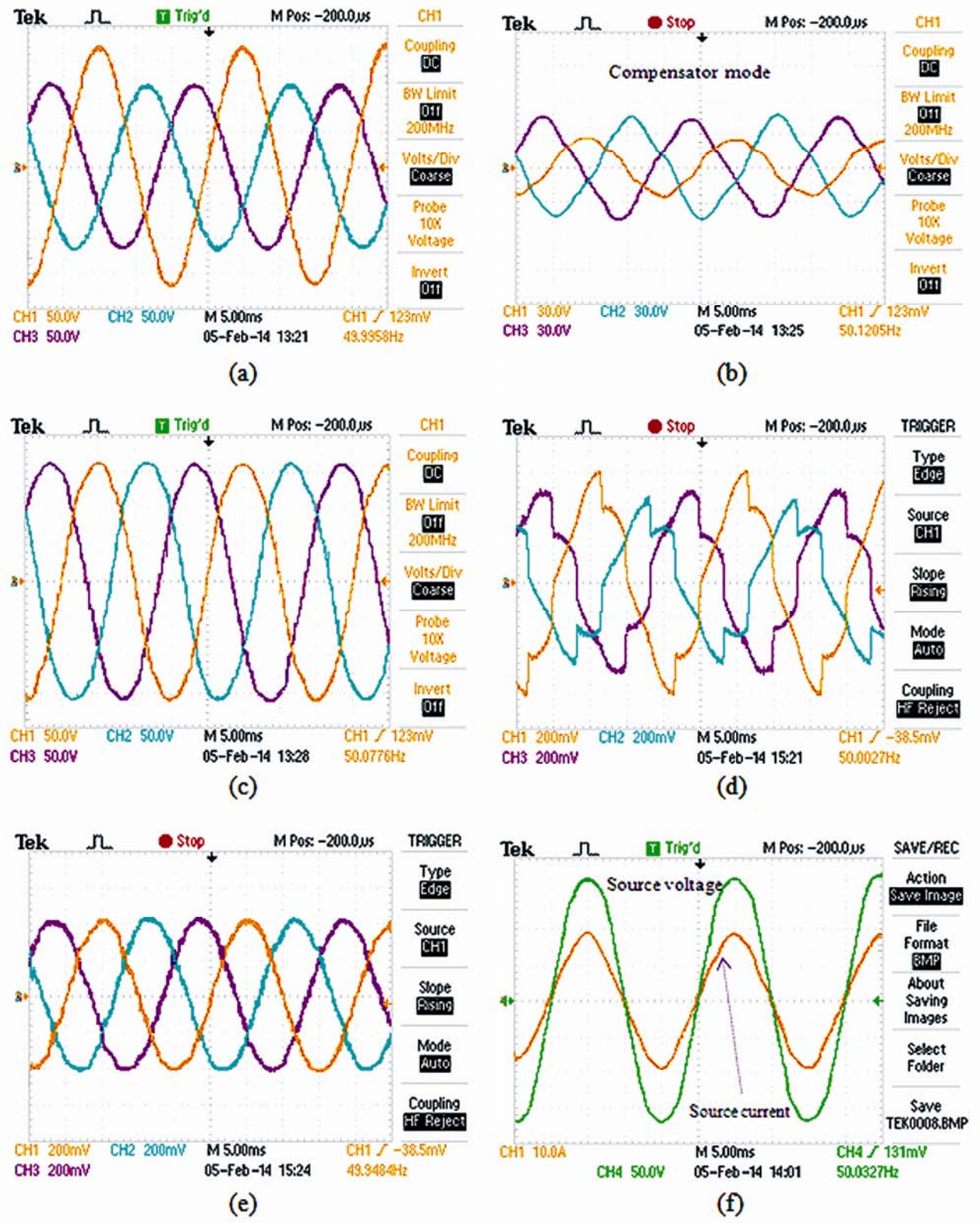

Fig. 13—Experimental results under balanced voltages with unbalanced loads: (a) source voltages (V_{sabc}) before compensation, (b) injected voltage, (c) Load voltage (V_{labc}) after compensation, (d) load currents (i_{labc}), (e) source currents (i_{sabc}) after compensation and (f) source voltage (V_{sa}) superimposed by the source current (i_{sa})

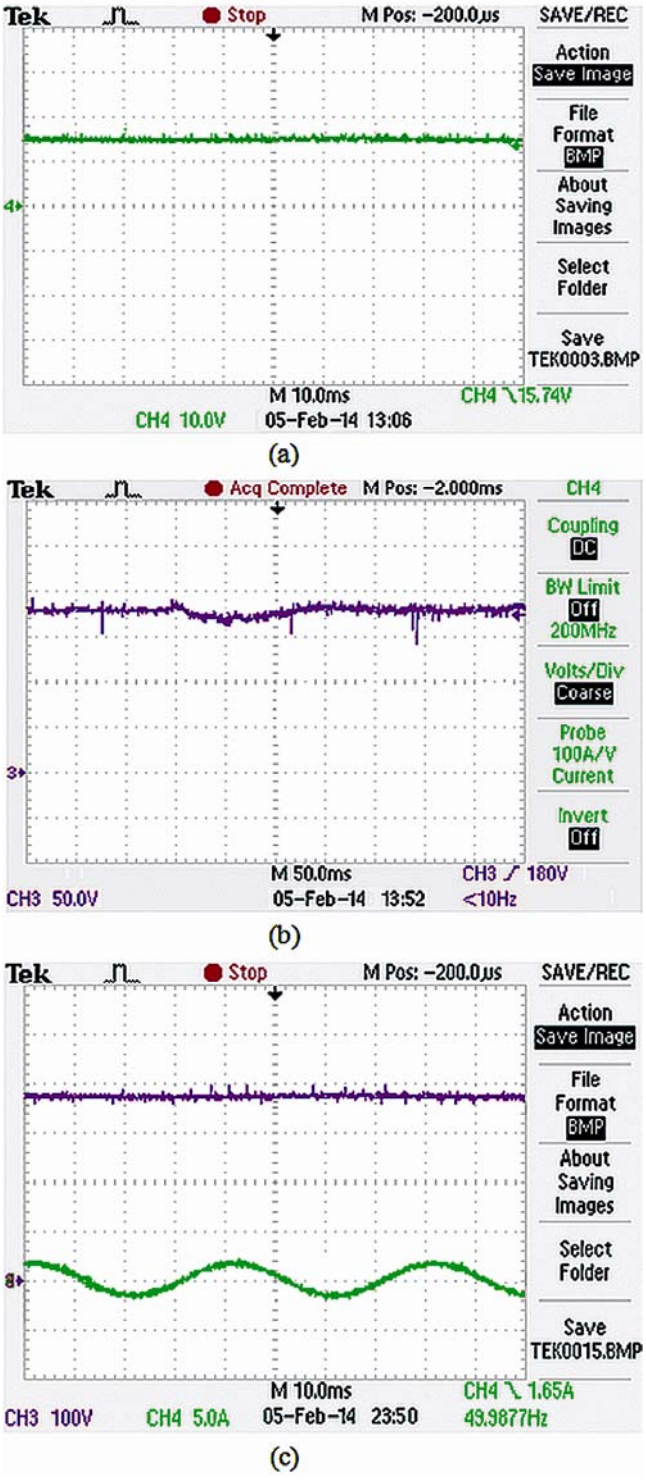

Fig. 14—PV array output voltage, high step-up DC-DC converter output voltage, DC-link capacitor voltage and neutral current after compensation

31.3%, 34.50% and 30.10%; and are reduced to 3.5%, 4.10% and 3.65% after compensation, respectively.

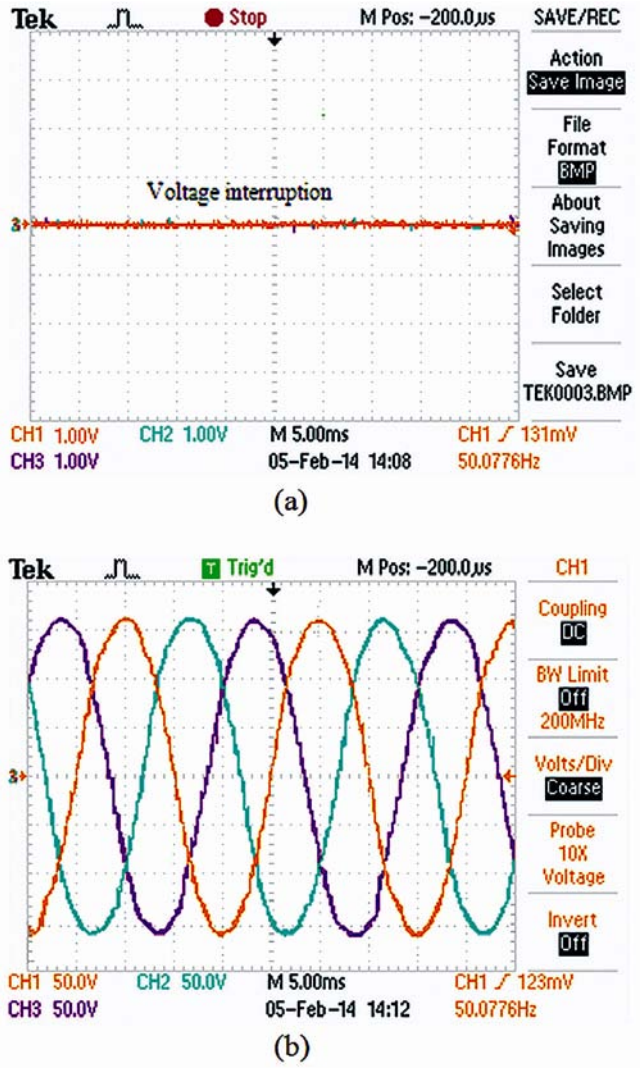

Fig. 15—Voltage interruption compensation (a) source voltage and (b) load voltage

Table 5—Experimental results in terms of THD levels of voltage and current waveforms at PCC

		Before PV based SHAPF		After PV based SHAPF	
	Phases	Currents (A)	Voltages (V)	Currents (A)	Voltages (V)
THD (%)	A	31.50	19.30	3.50	1.50
	B	34.50	23.20	4.10	2.00
	C	30.10	25.60	3.65	2.75

The compensation results of the experimental set-up are summarized in Table 5 in terms of THD levels of voltage and current wave forms.

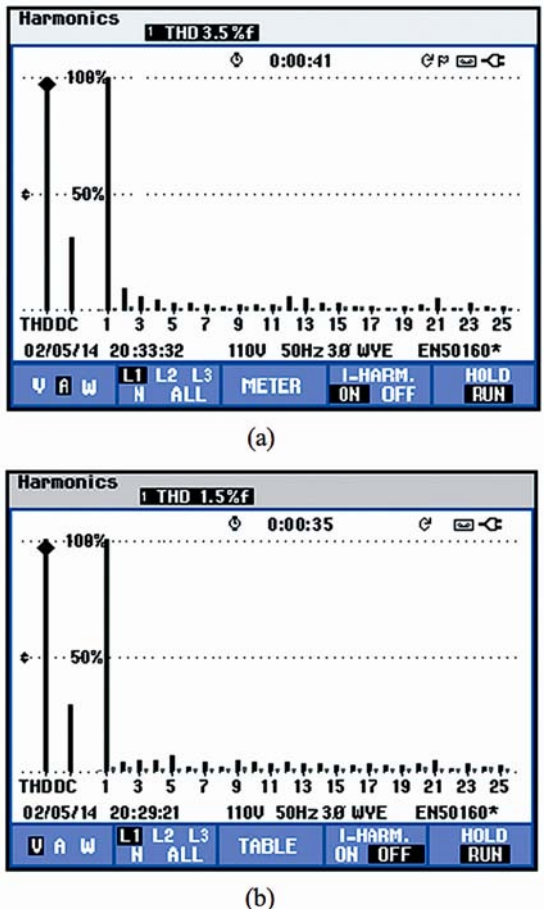

Fig. 16—THD level of source current and load volatage after compensation in phase-'*a*'

Conclusions

This paper investigates the proposed PV interfaced three-phase four-wire SHAPF to compensate the reactive power, harmonic current, voltage sags/swell, voltage imbalance and voltage interruption at residence or small industry. A DC-DC converter with P&O MPPT algorithm is implemented to track the maximum power point of the PV array. Additionally, adaptive fuzzy logic controller is introduced to adapt PI controller parameters K_p and K_i to control the DC-link voltage of the SAPF. This novel PV-SHAPF is designed to utilize the renewable energy accordingly saves the energy and shares the load during the solar irradiation available. The added advantages of the system are: reducing the panel tariff and avoiding the use of UPS and power quality conditioner for the individual equipment at a residence, small industry and educational institutions. The simulation and experimental results show the capability of PV-SHAPF in mitigating the voltage and current based distortions.

References

1 Akagi H, *IEEE Trans Ind Appl*, 32 (1996)1312-1322.
2 Singh B, Al-Haddad K & Chandra A, *IEEE Trans Ind Electron*, 46(5) (1999) 960-971.
3 Fujita H & Akagi H, *IEEE Trans Power Electron*, 22(3) (2007) 1046-1053.
4 Jindal A K, Ghosh A & Joshi A, *Elect Power Syst Res*, 73 (2005) 187-196.
5 Salmeron P & Litran S P, *IEEE Trans Power Delivery,* 25(2) (2010) 1058-1067.
6 Hamadi A, Rahmani S & Al-Haddad K, *IEEE Int Symp Ind Electron (ISIE-2009)*, (2009) 286-291.
7 Hamadi A, Rahmani S & Al-Haddad K, *IEEE Power Electron Specl Conf (PESC* '2007), (2007) 1099-1104,.
8 Bhattacharya S, Divan D M & Banerjee B B, *IEEE Power Electron. Specl Conf (PESC* '93), (1993) 779-786.
9 Dasgupta S, Mohan S N, Sahoo S K, Panda S K, *IEEE Trans Ind Electron*, 60(3) 92013) 1204-121.
10 Dasgupta S, Sahoo S K, Panda S K & Amaratunga G, *IEEE Trans Power Electron*, 26(3) (2011) 732-746.
11 Basu M, Das S P & Dubey G K, *IET Gener Trans Distrib,* 2(3) (2008) 414-423.
12 Cavalcanti M C, Azevedo G M S, Amaral B A & Neves F A S, *Industrial Electronics Society (IECON-2005) 31st Ann Conf IEEE*, (2005) 750-755.
13 Khadkikar V & Chandra A, *IEEE Trans Power Electron,* 26(9) (2011) 2414-2425.
14 Kumar G S, Kumar B K & Mishra M K, *IEEE Trans Power Deliv,* 26(4) (2011) 2761-2673.
15 Oliveira da Silva S A, Donoso-Garcia P, Cortizo P C & Seixas P F, *Int J Electr Power Energy Syst*, 26(6) (2004) 399-411.
16 Bose B K, *Proc IEEE*, 82(8) (1994) 1303-1323.
17 Jain S K, Agrawal P & Gupta H O, *Proc Inst Elect Eng, Electr Power Appl*, 149(5) (2002).
18 Saribulut L & Tumay M, *IEEE Trans Power Deliv,* 26(4) (2011) 2205-2214.
19 Routimo M, Salo M & Tuusa H, *IEEE Trans Power Electron*, 22 (2007) 636-643.
20 Ojo O & Kshirsagar P M, *IEEE Trans Power Electron*, 19(1) (2004) 46-53.
21 Singh B N, Rastgoufard P, Singh B, Chandra A & Haddad K Al, Design, *IEE Electric Power Appl,* 151(4) (2004) 467-476.
22 Kwon Jung-Min, Nam Kwang-Hee & Kwon Bong-Hwan, *IEEE Trans Ind Electron*, 53(4) (2006) 1048-1054.
23 Jiang Wei, Zhou Yu-Fei, Chen Jun-Ning, Modeling and Simulation of Boost Converter in CCM and DCM. *IEEE Conf* 2009, 288-291.
24 Hussein K H, Muta I, Hshino T & Osakada M, *Proc Inst Electr Eng*, 142(1) (1995) 59-64.
25 Esram T & Chapman P L, *IEEE Trans Energy Conv*, 22(2) (2007) 439-449.
26 Peng F Z & J S Lai, *IEEE Trans Instrum Meas*, 45 (1996) 293-297.
27 Akagi H, Watanabe E H & Aredes M, i*Instantaneous Power Theory and Applications to Power Condtioning*, (IEEE Press, Wiley), 2007.
28 Herrera R S & Salmerón P, *IEEE Trans Power Deliv,* 22(1) (2007) 595-604.
29 Salmerón P & Litrán S P, *IEEE Trans Power Electron*, 25(7) (2010) 1923-1931.